Activation of Peroxisome Proliferator Activator Receptor Delta in Mouse Impacts Lipid Composition and Placental Development at Early Stage of Gestation 1

Authors: Ding, Hongjuan, Zhang, Yiyu, Liu, Lun, Yuan, Hongyan, Qu, Jian, et al.

Source: Biology of Reproduction, 91(3)

Published By: Society for the Study of Reproduction

URL: https://doi.org/10.1095/biolreprod.113.116772

BIOLOGY OF REPRODUCTION (2014) **91**(3):57, 1–11
Published online before print 11 June 2014.
DOI 10.1095/biolreprod.113.116772

Activation of Peroxisome Proliferator Activator Receptor Delta in Mouse Impacts Lipid Composition and Placental Development at Early Stage of Gestation[1]

Hongjuan Ding,[3,4] Yiyu Zhang,[3,5] Lun Liu,[6] Hongyan Yuan,[4] Jian Qu,[4] and Rong Shen[2,7]

[4]*State Key Laboratory of Reproductive Medicine, Department of Obstetrics, Affiliated Nanjing Maternity and Child Health Care Hospital, Nanjing Medical University, Nanjing, China*
[5]*Johns Hopkins Bloomberg School of Public Health, Johns Hopkins University, Baltimore, Maryland*
[6]*Beijing Agriculture Institution, Beijing, China*
[7]*State Key Laboratory of Reproductive Medicine, Department of Oncology, Affiliated Nanjing Maternity and Child Health Care Hospital, Nanjing Medical University, Nanjing, China*

ABSTRACT

Peroxisome proliferator-activated receptor delta (*Ppard*) activation has been implicated in regulating a multitude of biological processes in placental development. In this study, we employed the UPLC-ESI-TOFMS approach to investigate the metabolic traits in placenta from GW501516-treated mice at Embryonic Day 10.5. By analyzing the mass spectrum data, ions with the most significant differences between control and GW501516-treated groups were identified. Among these metabolites, the fatty acids, phospholipids, and sterol lipids were dramatically increased. Ingenuity Pathway Analysis (IPA) showed that phosphatidylethanolamine biosynthesis and glycolysis were the top two altered metabolic pathways involved in carbohydrate metabolism, energy production, and lipid metabolism. Subsequent immunoblotting experiments provided evidence for positive correlation of PPARD level and AKT and ERK signaling pathways upon GW501516 treatment. Furthermore, the stimulation of GW501516 increased trophoblast cell fusion gene syncytin-A (*Syna*), but not syncytin-B (*Synb*), expression, suggesting a potential role of *Ppard* activation in promoting cytotrophoblast differentiation. Our results reveal that *Ppard* activation elicits dramatic changes of the metabolic activities in placenta, which is correlated to AKT and ERK signaling.

metabolism, peroxisome proliferator activator receptor delta, placenta, Ppard, *pregnancy, signaling pathway, UPLC-ESI-TOFMS approach*

INTRODUCTION

The placenta is the first fetal organ to form during mammalian embryogenesis [1–3]. During gestation, the major function of placenta is to produce hormones, synthesize and release fatty acid, and facilitate efficient nutrient uptake [4–6]. A number of transcription factors have been implicated in placental development [7–9]; however, it remains unclear which factor is essential for this biological process.

Peroxisome proliferator-activated receptors (PPARs) are a family of the nuclear hormone receptors belonging to the steroid receptor superfamily. PPARs function as gene transcription factors in controlling lipid metabolism, energy homeostasis, and cell differentiation. The three subtypes have been described as *Pparα*, *Ppard*, and *Pparg* [10]. Each PPAR isotype has distinct tissue distributions, physiological functions, and ligands.

Among these three isotypes, *Ppard* is the most important regulator for executing key cellular functions in heart, liver, colon, and skeletal muscle. Physically, *Ppard* is activated by a large spectrum of endogenous and synthetic ligands, such as fatty acids, eicosanoids, prostacyclin, and GW501516 [11–13]. *Ppard* activation elicits multiple metabolic responses found in vitro and in vivo, which include improving lipid oxidation and glucose uptake in skeletal muscle [14], stimulating lipid accumulation in keratinocytes [15], and increasing transintestinal cholesterol efflux [16]. *Ppard* activation has also been involved in cell differentiation [17], proliferation [18], and inflammation [19]. As a result, *Ppard* has been recognized as a major regulator in determining cell fate and a promising target in treatment of metabolic diseases [20].

In placenta, *Ppard* is the most ubiquitously expressed PPAR subtype in the early stage of pregnancy [21]. In particular, PPARD is more pronounced in the syncytiotrophoblast of human placenta [22]. A number of studies in *Ppard*-null mice have revealed that *Ppard* is involved in several aspects of placentation processes, including blastocyst implantation and decidualization, and is also critical for the integrity of the placenta-decidua interface [23, 24]. Loss of *Ppard* in mice confers placental defects, leading to more than 90% embryonic lethality between Embryonic Day (E) 9.5 and E10.5 [25], whereas activation of *Ppard* triggers massive trophoblastic giant cell differentiation with increased ADRP expression [26]. This implies that *Ppard* is a key regulator in placental metabolism and endocrine activities. PPARD agonist exposure has also been reported to negatively regulate phospholipids, cholesteryl esters, and cholesterol concentrations in normal human placenta [27, 28].

Considering the majority of placental *Ppard*-dependent metabolites have not been described as *Ppard* targets in placenta, the present study undertakes a metabolomics approach aimed to elucidate the specific metabolic and molecular pathways of *Ppard* activation in placental development upon *Ppard* agonist treatment.

[1]Supported by grant SKLRM-KF-1206 from State Key Laboratory of Reproductive Medicine and by grant YKK07056 from Nanjing Science and Technology Foundation, Nanjing, China.
[2]Correspondence: Rong Shen, State Key Laboratory of Reproductive Medicine, Department of Oncology, Affiliated Nanjing Maternity and Child Health Care Hospital, Nanjing Medical University, 123 Tianfei Rd, Nanjing 201300, China. E-mail: drrongshen@gmail.com
[3]These authors contributed equally to the work.

Received: 29 December 2013.
First decision: 23 January 2014.
Accepted: 22 May 2014.

eISSN: 1529-7268 http://www.biolreprod.org
ISSN: 0006-3363

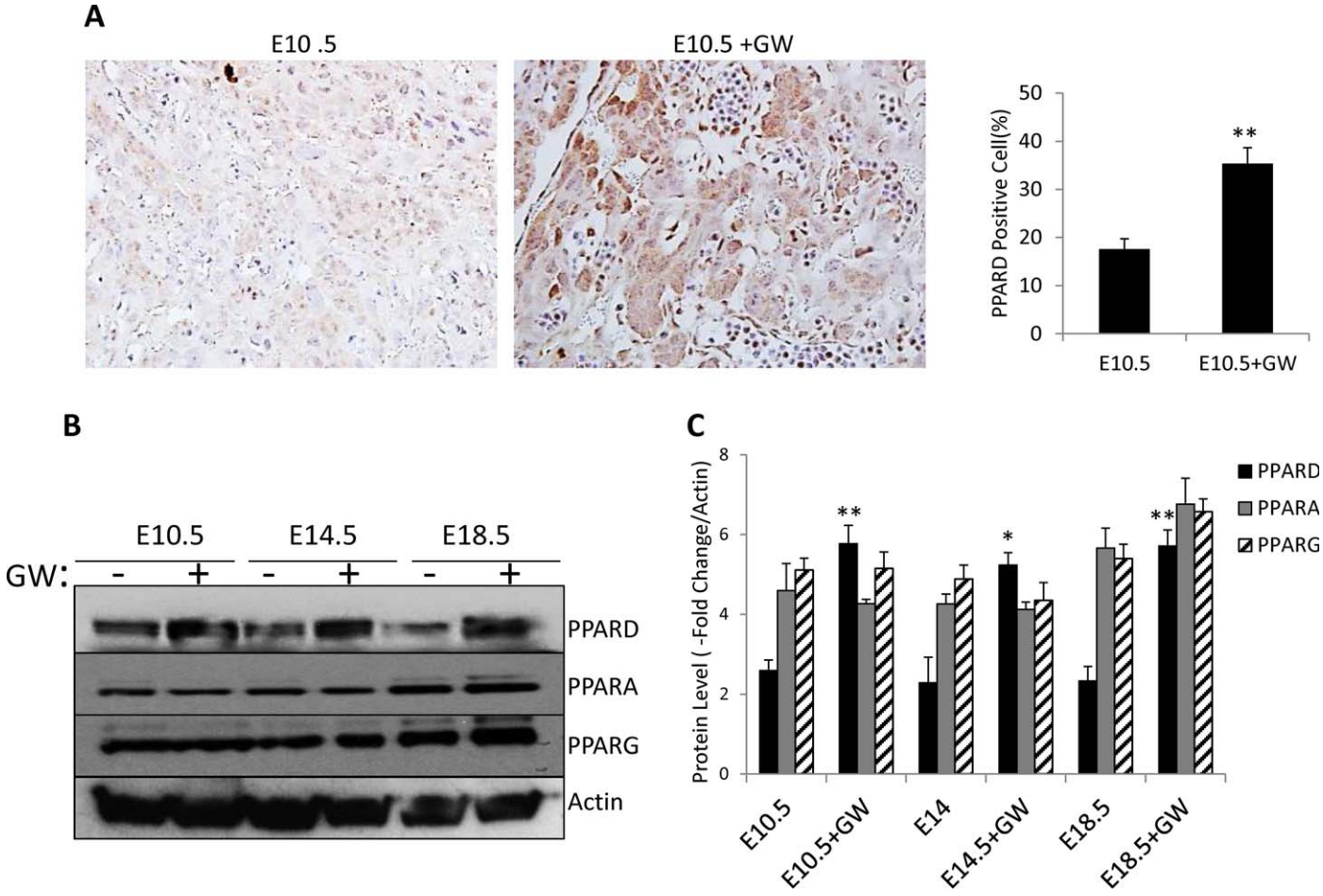

FIG. 1. The effects of *Ppard* agonist on mouse placenta. **A**) Immunohistochemical analysis indicated that PPARD is expressed in syncytiotrophoblast cells and increased in response to GW501516. Representative images from control and GW501516-treated mice are shown. Bar graph indicates the number of PPARD-positive cells per 1000 cells based on a total of six samples. $^{**}P < 0.01$, Student *t*-test. Magnification ×400. **B** and **C**) Representative Western blots (**B**) and quantification (**C**) of PPARA, PPARG, and PPARD protein expression in mice from E10.5 (n = 6), E14.5 (n = 4), and E18.5 (n = 5) placenta. All values are normalized to actin. Each value represents the mean ± SD, expressed relative to control values. Student *t*-test was performed on the data. $^{**}P < 0.01$, $^{*}P < 0.05$ denotes significant differences between GW501516-treated and control groups.

MATERIALS AND METHODS

All protocols were approved by the Institutional Animal Care and Use Committee at Nanjing Medical University.

Animal

Female FVB mice were fed with the standard lab chow diet (3.1 kcal/g, containing 58% carbohydrate, 25% protein, and 12% fat; the diet was formulated in the laboratory) and water after weaning. Pregnancy was produced at 6 wk of age by overnight caging of a fertile female with a fertile male mouse. The next morning, the presence of a vaginal plug was defined as E0.5. Pregnant mice were randomized in two groups. Mice were orally administered vehicle (0.5% w/v aqueous methylcellulose solution) or a selective *Ppard* activator, GW501516 (kindly provided by Dr. Xirong Guo, Nanjing Medical University), at a dose of 2 mg/kg/day. Cesarean section was performed to collect both groups of placenta at E10.5 (n = 6 per group), E14.5 (n = 4 per group), and E18.5 (n = 4 per group). Samples were either frozen in liquid nitrogen or fixed in 10% formalin for further analysis.

Histopathology and Immunohistology

To investigate whether daily oral administration of GW501516 leads to morphological changes, placentas were collected at E10.5, E14.5 and E18.5, then sectioned and sequentially analyzed by histology. Immunohistochemistry was carried out on sections using the avidin-biotin-peroxidase method (Vector Laboratories) on 7-μm sagittal placental Paraffin-embedded sections. Endogenous peroxidases were quenched by exposing the sections to 3% H_2O_2 for 5 min, followed by a wash in PBS. Nonspecific binding sites were blocked by using 10% normal goat serum with 0.1% Triton-100 in PBS for 1 h. The sections were incubated with the primary antibody (see Supplemental Table S1; supplemental data are available online at www.biolreprod.org) overnight at 4°C. Slides were washed with PBS and incubated with appropriate biotinylated secondary antibodies (1:200; Vector Laboratories) for 45 min, followed by 30-min incubation in an avidin-biotin complex solution (Vector Laboratories). After washing three times in PBS, the sections were stained with peroxidase substrate solution until the desired stain intensity developed and then counterstained with hematoxylin solution for 5 min. Sections were mounted in Permount mounting media. The negative-control slides (immunoglobulin G only) were included in every individual analysis. Six mice in each group were used for quantification. Three high-power fields (400×) were randomly chosen for counting PPARD-immunostained cells in each sample. Approximately 1000 cells per group were analyzed. Student *t*-test was used to determine the level of significance ($P < 0.05$) between two groups. Data are presented as the mean ± SD.

Western Blot Analysis

The placentas were frozen in liquid nitrogen and pulverized in a mortar and pestle, then mixed with lysis buffer containing 50 mM Tris-HCl (pH 7.5), 0.5% NP-40, 0.1% SDS, 0.25% sodium deoxycholate, 125 mM NaCl, 1 mM ethylenediaminetetra-acetic acid, 50 mM NaF, 1 mM sodium orthovanadate, 2.5 mM sodium pyrophosphate, 1 mM sodium β-glycerophosphate, 1 mM PMSF, and protease inhibitor cocktail (Roche Diagnostics). Following incubation on ice for 30 min, the lysates were cleared by centrifugation at 13 000 × *g* for 15 min at 4°C. Protein concentrations were determined by

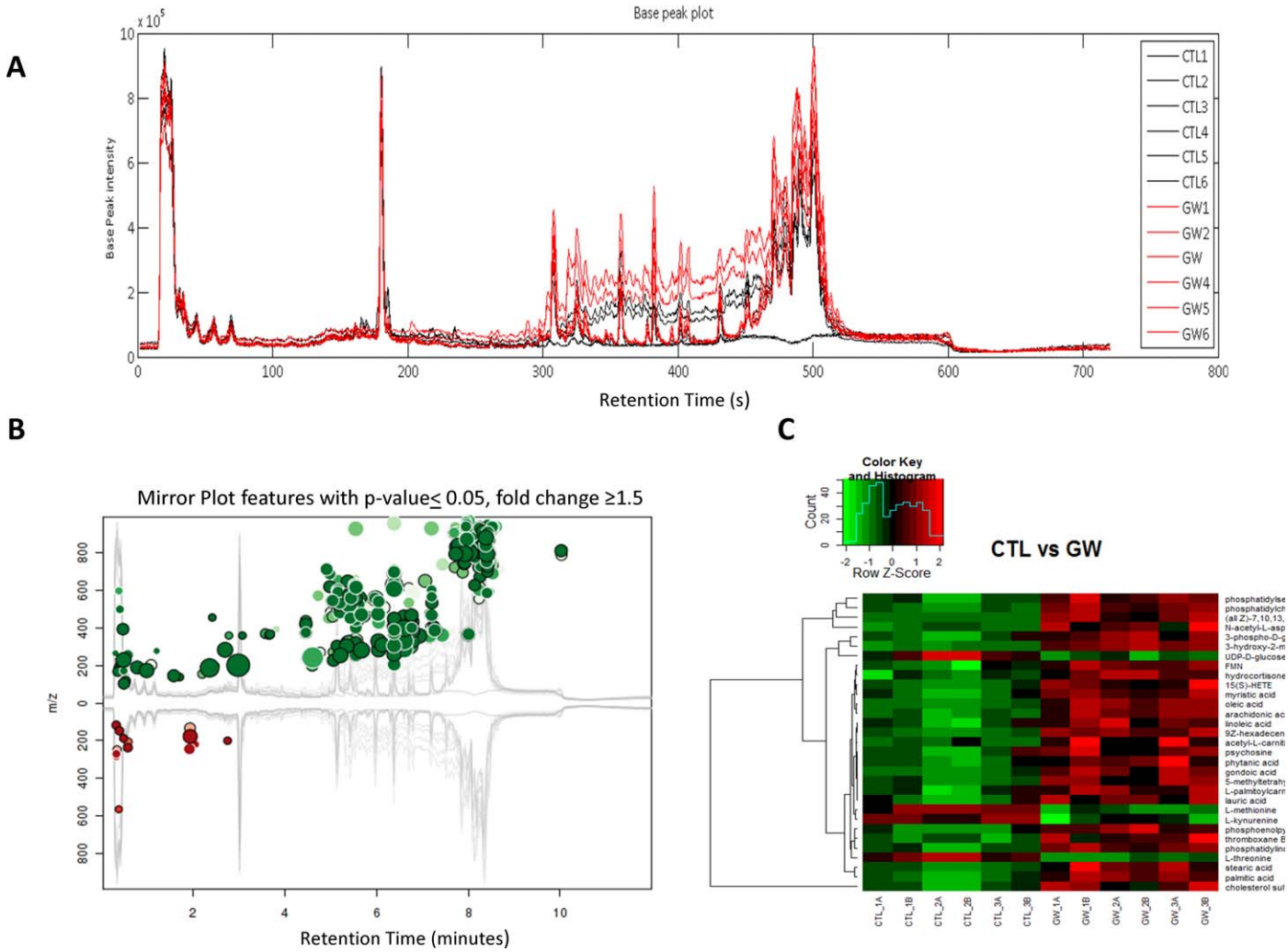

FIG. 2. UPLC-ESI-TOF-MS profiling of metabolites altered in placenta. In all, 561 metabolites for which expression was altered more than 1.5-fold were applied to IPA. **A**) Base peak plot shows the overlay of total ion chromatograms of GW501516-treated group (red) and control group (black). **B**) Mirror plot of placenta differential metabolites. Up-regulated features are shown in green and down-regulated features in red. **C**) Heat map depicts the changes of metabolites for control and GW501516-treated placenta (n = 6 individual measurements per group).

Coomassie Plus Protein Assay (Pierce), and then 50 μg of lysate were separated in a 4%–12% NuPAGE Bis-Tris gel (Invitrogen). After wet transfer, membranes were blocked for 1 h at room temperature in Tris-buffered saline (pH 7.4) containing 5% nonfat dry milk and 0.1% Tween 20, then incubated with appropriate primary antibody (see Supplemental Table S1) overnight at 4°C and horseradish peroxidase-linked secondary antibodies for 1 h at room temperature. Proteins were visualized with either SuperSignal West Pico or SuperSignal West Dura (Pierce). The band intensity was quantified by Scion Image software. Band intensity was normalized to total protein or actin in respective columns. Wilcoxon rank-sum test was used to determine the level of significance ($P < 0.05$) between two groups. Results are presented as the mean ± SD from three separate experiments.

Sample Preparation and Mass Spectral Analysis

To gain further understanding of the effect of GW501516, we measured the mouse placental metabolism at E10.5 by using the ultraperformance liquid chromatography (UPLC) and the accurate mass measurement of electrospray ionization time-of-flight mass spectrometry (ESI-TOFMS) approach. Cold methanol extracts of placentas from six controls and an equal number of mice treated with GW501516 for 10 days were applied for liquid chromatography (LC)-MS analysis. Samples were clarified and processed as described below: Each sample (5 μl) was injected onto a reverse-phase 50- × 2.1-mm ACQUITY 1.7-μm C18 column (Waters Corp.) using the ACQUITY UPLC System (Waters) with a gradient mobile phase consisting of 2% acetonitrile in water containing 0.1% formic acid (A) or 2% water in acetonitrile containing 0.1% formic acid (B). Each sample was resolved for 10 min at a flow rate of 0.5 ml/min. The gradient consisted of 100% A for 0.5 min, then a ramp of curve 6 to 100% B from 0.5 to 10 min. The column eluent was introduced directly into the mass spectrometer by electrospray. The desolation gas flow was set to 800 L/h, and the temperature was set to 350°C. The cone gas flow was 25 L/h, with a source temperature of 120°C. Accurate mass was maintained by introduction of LockSpray interface of leucine-enkephalin (556.2771 $[M+H]^+$ or 554.2615 $[M-H]^-$) at a concentration of 2 ng/μl in 50% aqueous ACN with an infusion rate of 2 μl/min for the positive mode and 3 μl/min for the negative mode.

Metabolites Identification and Data Preprocessing

The UPLC-ESI-TOFMS data in positive and negative modes were analyzed by the MassLynx software (Waters) with the format of Network Common Data Form. Then, XCMS Online [29] was used for candidate identification. The parameter was optimized with UPLC/Q-TOF high-resolution LC-MS data according to Patti et al. [30]. The ions with a fold-change larger than 1.5 and a *P*-value less than 0.05 were selected for further analysis. Total ion chromatograms plot, mirror plot, and principal components analysis results were provided by XCMS Online. Boxplot and extracted-ion chromatogram peaks were also generated by XCMS Online and sorted in the order of most to least significant. Putative identifications for the resulting ion list were obtained through a database search tool [31] that combines the following four metabolite identification databases (Human Metabolite DataBase [32], Metlin [33], Madison Metabolomics Consortium Database [34], and LIPID MAPS [35]) with mass tolerance set to 10 ppm. For metabolite statistical analysis, R scripts developed in-house were used to select the ions with significant and consistent changes between the treated and control groups. To delineate the early

TABLE 1. The most relevant metabolites identified in the GW501516-treated group compared to control group.

Symbol	KEGG[a]	Fold-change	*P*-value
(all Z)-7,10,13,16,19-docosapentaenoic acid	C16513	16.603	8.51E-04
Eicosapentaenoic acid	C16184	16.603	8.51E-04
cis-11,14,17-Eicosatrienoic acid	C16522	11.164	3.72E-03
8Z,11Z,14Z-Eicosatrienoic acid	C03242	11.164	3.72E-03
Vaccenic acid	C08367	8.03	6.51E-06
6Z-octadecenoic acid	C08363	8.03	6.51E-06
Elaidic acid	C01712	8.03	6.51E-06
Oleic acid	C00712	8.03	6.51E-06
Phosphatidylethanolamine	C00350	7.169	8.72E-05
Phosphatidylcholine	C00157	7.169	8.72E-05
Triamcinolone hexacetonide	C08185	6.815	3.49E-04
9Z-hexadecenoic acid	C08362	6.009	2.37E-06
Gondoic acid	C16526	5.721	1.89E-04
Methandriol	C14493	5.674	1.67E-04
Arachidonic acid	C00219	5.674	1.67E-04
Stearic acid	C01530	5.397	8.67E-04
5-Methyltetrahydrofolic acid	C00440	5.275	9.22E-04
12(R)-hydroxyeicosatetraenoic acid	C14822	5.111	3.42E-03
12(S)-hydroxyeicosatetraenoic acid	C14777	5.111	3.42E-03
8(S)-hydroxyeicosatetraenoic acid	C14776	5.111	3.42E-03
14,15-Epoxyeicosatrienoic acid	C14771	5.111	3.42E-03
11,12-Epoxyeicosatrienoic acid	C14770	5.111	3.42E-03
8,9-Epoxyeicosatrienoic acid	C14769	5.111	3.42E-03
5,6-Epoxyeicosatrienoic acid	C14768	5.111	3.42E-03
20-Hydroxyeicosatetraenoic acid	C14748	5.111	3.42E-03
5(S)-HETE	C04805	5.111	3.42E-03
15(S)-HETE	C04742	5.111	3.42E-03
Nervonic acid	C08323	4.609	2.79E-04
Palmitic acid	C00249	4.134	7.22E-05
Deoxycorticosterone acetate	C14554	4.077	7.43E-05
Phosphatidylserine	C02737	3.825	1.44E-04
Phosphatidylinositol	C00626	3.599	1.24E-04
Cholesterol sulfate	C18043	3.424	1.74E-03
Myristic acid	C06424	3.284	4.47E-04
5beta-Tetrahydrocorticosterone	C05476	3.249	2.92E-03
Arachidic acid	C06425	3.208	2.36E-03
Phytanic acid	C01607	3.208	2.36E-03
Lauric acid	C02679	2.874	3.61E-03
Psychosine	C01747	2.733	4.05E-03
(S)-3-hydroxy-2-methylpropanoic acid	C06001	2.723	4.36E-07
3-Hydroxy-2-methylpropanoic acid	C01188	2.723	4.36E-07
(R)-3-hydroxybutyric acid	C01089	2.723	4.36E-07
4-Hydroxybutanoic acid	C00989	2.723	4.36E-07
Acetyl-L-carnitine	C02571	2.658	8.68E-03
L-Palmitoylcarnitine	C02990	2.593	2.84E-03
9Z,11E-octadecadienoic acid	C04056	2.525	3.65E-03
Linoleic acid	C01595	2.525	3.65E-03
N-acetyl-L-aspartic acid	C01042	2.325	5.46E-03
Thromboxane B2	C05963	2.226	3.48E-03
Clavulanic acid	C06662	2.168	9.35E-03
Phosphoenolpyruvate	C00074	2.161	5.30E-04
Omega-hydroxypalmitic acid	C18218	2.053	4.53E-03
Tetrahydrocortisol	C05472	1.983	2.83E-04
18-Hydroxycorticosterone	C01124	1.778	8.23E-04
Hydrocortisone	C00735	1.778	8.23E-04
Nitrendipine	C07713	1.611	2.77E-04
FMN	C00061	1.577	1.44E-03
2-Phospho-D-glycerate	C00631	1.546	1.90E-03
3-Phospho-D-glycerate	C00197	1.546	1.90E-03
UDP-D-galactose	C00052	−1.503	2.66E-03
UDP-D-glucose	C00029	−1.503	2.66E-03
L-Kynurenine	C00328	−1.687	4.28E-03
L-Threonine	C00188	−1.81	9.59E-05
Naltrexone	C07253	−1.914	5.54E-03
Ketorolac	C07062	−2.149	3.65E-03
Magnolol	C10651	−2.739	1.26E-03
Honokiol	C10630	−2.739	1.26E-03

[a]KEGG, Kyoto Encyclopedia of Genes and Genomes.

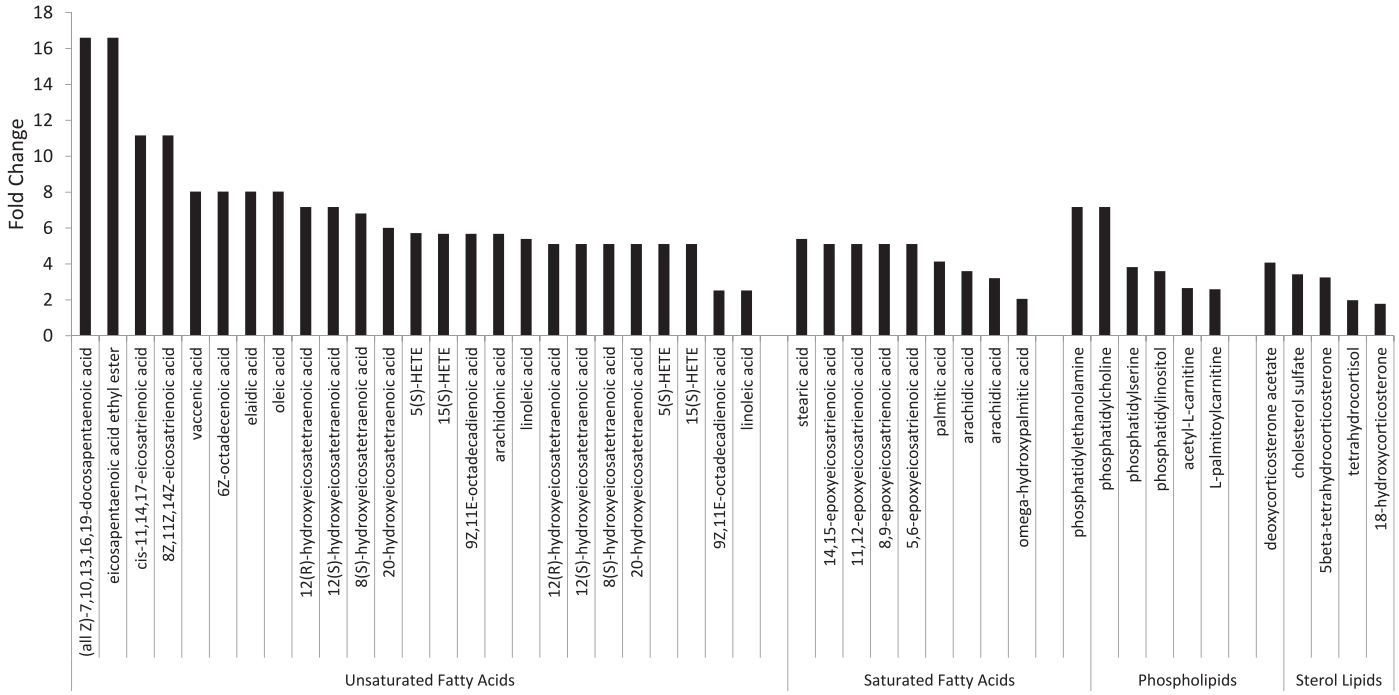

FIG. 3. Analysis of lipids composition in GW501516-treated group compared to control group.

metabolic consequences of *Ppard* activation, metabolomics analysis was carried out with extracts (n = 6 per group) from control and GW501516-treated placenta based on one-way ANOVA and the variability of the corresponding peaks in the quality control runs of the placental samples.

Quantitative Real-Time PCR

Total RNA was extracted using TRIzol (Sigma) from E10.5 placentas following the manufacturer's protocol. One microgram of RNA was reverse transcribed in a total volume of 20 µl using the Omniscript Reverse Transcription Kit (Qiagen). Quantitative real-time PCR (qPCR) was performed with the primers CTGGGAATATGAACCCACTGTTA and GAGTTGAGG CAGAAGGAGTATG for syncytin-A (*Syna*) and the primers CCACCACC CATACGTTCAAA and GGTTATAGCAGGTGCCGAAG for syncytin-B (*Synb*). The qPCRs were performed in triplicate in an ABI Prism 7700 Instrument (Applied Biosystems) with QuantiTect SYBR Green (Qiagen) following the manufacturer's protocol. The PCR products were confirmed by ethidium bromide staining on a 2% agarose gel. The expression of each target gene was presented as the ratio of the target gene to 18S RNA, which was expressed as $2^{-\Delta Ct}$, where Ct is the threshold cycle and $\Delta Ct = Ct^{Target} - Ct^{18S}$. Students *t*-test was applied to determine the level of significance ($P < 0.05$) between two groups. Values represent the mean ± SD from three separate experiments.

Molecular Pathway and Network Analysis by Ingenuity Pathway Analysis

Ingenuity Pathway Analysis (IPA) was applied to identify biological pathways and functions relevant to biomolecules of interest. A ratio of metabolites that map to the pathways divided by the total number of molecules that map to canonical pathways was displayed. Fisher exact test was adapted to calculate the *P*-value determining the probability that the association between the metabolites and the canonical pathway was explained by chance alone. The network score was based on the hypergeometric distribution and was calculated by two-tailed Fisher exact test. The higher the score, the more relevant the eligible submitted molecules were to the network.

RESULTS

Histologic Analysis of Ppard *Agonist Effects on Mouse Placenta*

Histologic analysis indicated no significant placental morphologic change between the GW501516-treated group and the control group at E10.5 (Supplemental Fig. S1) or at E14.5 and E18.5 (data not shown). We investigated the temporal/spatial pattern of PPARD expression in mouse placenta of E10.5. PPARD was predominantly expressed in syncytiotrophoblast in the labyrinth zone. GW501516-treated placenta showed a greater number of PPARD-positive cells than control placenta ($P < 0.01$) (Fig. 1A). Western blots were performed for PPAR protein expression analysis on placentas at E10.5, E14.5, and E18.5. GW501516 treatment induced detectable increase of endogenous PPARD protein expression, whereas PPARA and PPARG levels were not affected by GW501516 (Fig. 1B). PPARD protein levels were significantly increased in GW501516-treated mice at E10.5 ($P < 0.01$) (Fig. 1C).

Analysis of Global Metabolic Response of Placenta to Ppard *Agonist*

To evaluate if the UPLC-ESI-TOFMS-based metabolomics approach is useful to discriminate GW501516-treated placentas from controls (n = 6 per group), placental extracts were profiled using UPLC-ESI-TOFMS in positive mode and native mode, with the data preprocessed by XCMS. We detected 531 m/z chemically identified monoisotopic ion masses with significant difference in the treated group versus the control group (fold-change ≥ 1.5, $P < 0.05$). The base peak plot (Fig. 2A), mirror plot (Fig. 2B), and heatmap visualization (Fig. 2C) showed distinct segregation between GW501516 treatment and controls.

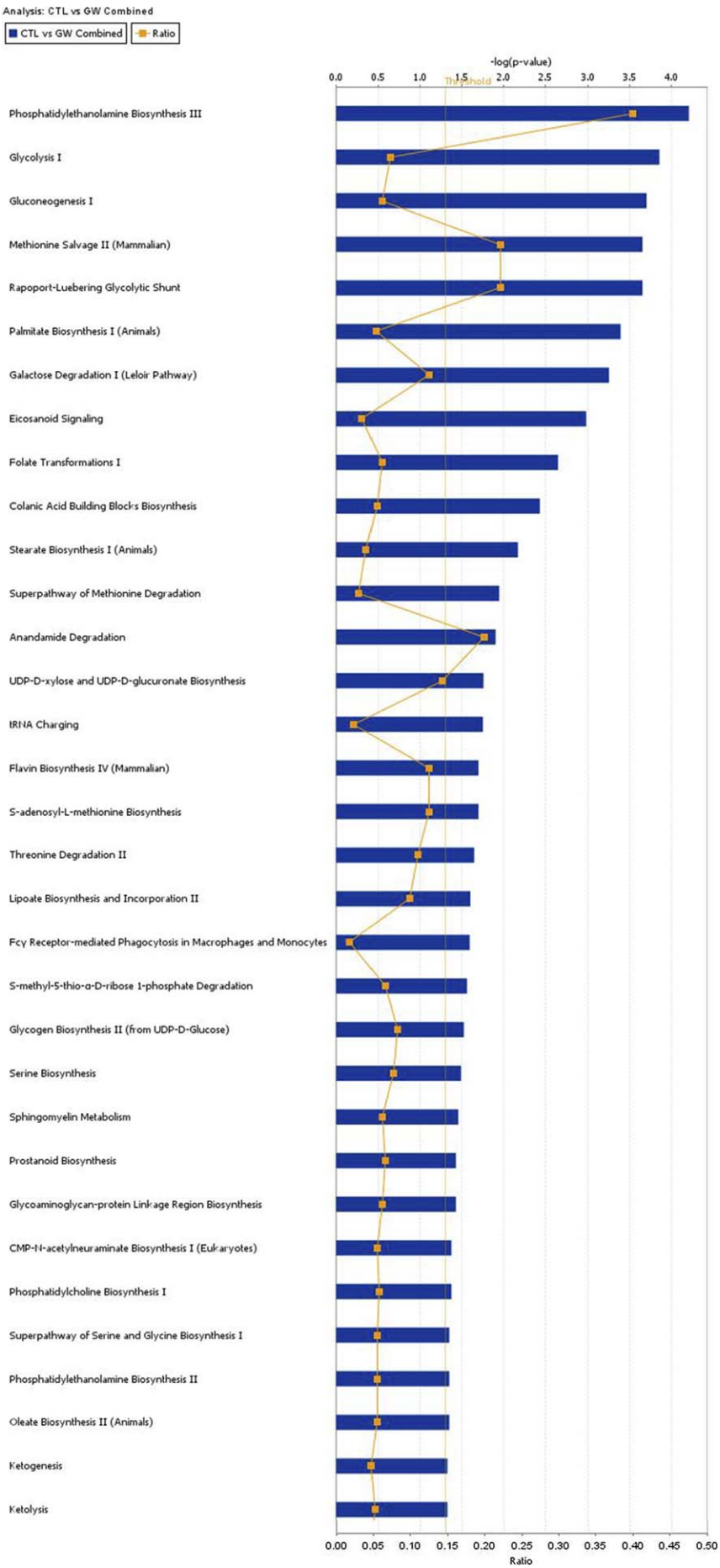

TABLE 2. IPA for metabolites in top related network and functions are listed.

ID	Molecules in network	Score	Focus molecules	Top functions
1	8,9-Epoxyeicosatrienoic acid, 11,12-epoxyeicosatrienoic acid, 14,15-epoxyeicosatrienoic acid, 20-hydroxyeicosatetraenoic acid, acetyl-L-carnitine, Acox, ADRB, arachidonic acid, cholesterol sulfate, CPT1, CYP4A, cytochrome *c*, elaidic acid, ERK1/2, gondoic acid, HDL, L-methionine, lauric acid, Ldh, linoleic acid, myristic acid, Nr1h, oleic acid, palmitic acid, phosphatidylcholine, phytanic acid, PP2A, proinsulin, psychosine, sPla2, stearic acid, thromboxane B2	48	20	Carbohydrate metabolism, energy production, and endocrine system development and function
2	2-Phospho-D-glycerate, 3-hydroxy-2-methylpropanoic acid, 3-phospho-D-glycerate, 5,6-epoxyeicosatrienoic acid, 5-hydroxyeicosatetraenoic acid, 5-methyltetrahydrofolic acid, 6Z-octadecenoic acid, 9Z-hexadecenoic acid, 12(R)-hydroxyeicosatetraenoic acid, 18-hydroxycorticosterone, (all Z)-7,10,13,16,19-docosapentaenoic acid, ADH5, alpha-ketoisocaproic acid, APP, Ca^{2+}, CERK, CYB5A, CYP11B2, FMN, gamma-linolenic acid, heme, L-kynurenine, L-palmitoylcarnitine, LCAT, LYPLA2, N-acetyl-L-aspartic acid, Na-K-ATPase, phosphoenolpyruvate, PKM, quinolinic acid, SLC22A6, SP1	32	15	Cell signaling and vitamin and mineral metabolism
3	5(S)-HETE,13(S)-hydroxyoctadecadienoic acid, 15(S)-HETE, AKT, collagen(s), ERK, focal adhesion kinase, Gsk3, Hsp70, hydrocortisone, IL1, IL12 (complex), Insulin, Jnk, L-threonine, MAPK, MAS1, NFkB (complex), Pate4, phosphatidylethanolamine, phosphatidylinositol, phosphatidylserine, PI3K	15	8	Lipid metabolism, small molecule biochemistry, and cellular assembly and organization

Identification of Metabolites Affected by Ppard *Agonist*

Table 1 presents the most relevant metabolites identified from these monoisotopic ion masses in distinguishing the treated group from the control group. The change of a metabolite is indicated with an average fold-change value. In all, 59 of 67 metabolites listed in Table 1 were up-regulated, and 8 of 67 metabolites were down-regulated, in response to GW501516. The metabolites of GW501516-treated mice, in comparison to those of control mice, exhibited an increase in fatty acid and phospholipid levels of eicosatrienoic acid (11.1-fold), (all Z)-7,10,13,16,19-docosapentaenoic acid (DPA; 16.6-fold), eicosapentaenoic acid (EPA; 16.6-fold), phosphatidylcholine (7.1-fold), phosphatidylethanolamine (PE; 7.1-fold), elaidic acid (8.0-fold), and arachidonic acid (AA; 5.674-fold), whereas the levels of L-threonine (−1.8 fold), sebacic acid (−1.6 fold), magnolol (−2.79 fold), and honokiol (−2.79 fold) were decreased in response to GW501516. As shown in Figure 3, an overall change in lipid composition in response to GW501516 was the significant increase of fatty acids, phospholipids, and sterol lipids.

Metabolic Pathway and Function Analysis

The 67 identified and quantified metabolites were applied to IPA. Figure 4 presents the top canonical pathways enriched in the metabolites identified with GW501516 in placenta, including PE biosynthesis and glycolysis. As shown in Table 2, network analysis of 67 differentially expressed metabolites revealed three significantly altered metabolism networks, including the key metabolites DPA, AA, PE, and 15(S)-HETE (Table 2). These metabolic networks were mainly involved in the following metabolite subset functions: 1) carbohydrate metabolism, energy production, and endocrine system development and function; 2) cell signaling and vitamin and mineral metabolism; and 3) lipid metabolism, small molecule biochemistry, and cellular assembly and organization.

Role of Ppard *Activation on AKT and ERK Cell Signaling Pathways*

The mechanistic network function analysis of IPA showed that AKT and ERK signaling pathways were predicted to be activated in response to GW501516 (Fig. 5). For further verification, Western blot analysis was conducted with mouse placenta tissues. As shown in Figure 6A, GW501516 treatment dramatically increased pTh308AKT ($^*P < 0.05$), pSer473AKT ($^*P < 0.05$), and pERK1/2 ($^*P < 0.05$) levels at E10.5 compared to the untreated group (Fig. 6B).

Role of Ppard *Activation on Placental* Syn *Expression*

Syna and *Synb* were used to evaluate the effect of *Ppard* activation on placental function. *Syn*a, but not *Synb,* was significantly increased ($P < 0.01$) in the GW501516-treated group compared to the control group (Fig. 7). This indicates that *Ppard* activation may enhance cytotrophoblast differentiation by inducing *Syna* expression.

DISCUSSION

The placenta is a prominent organ for glucose transport, fatty acid synthesis, and uptake for fetal growth and development. The metabolic activities in placenta are important for nutrient transport [36, 37]. In the present study, we characterized the metabolic changes pertaining to *Ppard* activation using the UPLC-ESI-TOFMS approach and function enrichment analysis. Our results indicate that placenta treated with GW501516 does not exhibit phenotype changes throughout pregnancy, which is different from the results of Nishimura et al. [38]. The use of different dosages of GW501516 (2 vs. 100 mg/kg/day) and different models (mice vs. rats) may have contributed to this difference.

The temporal/spatial expression patterns of PPARD suggest that oral GW501516 administration may have a direct influence on placenta. Our PPAR expression results indicate that PPARA and PPARG expression was not altered by GW501516, because GW501516 is the most potent PPARD

FIG. 4. Metabolites from the GW501516-treated group at E10.5 were associated with 33 distinctly different canonical pathways identified by IPA ($P < 0.05$). The *y*-axis represents the –log of *P*-values calculated by Fischer exact test. A threshold of $P = 0.05$ is represented by the light yellow line. This gives a measure for the possible impact of GW501516 on each listed pathway. The orange line represents the proportion of the amount of metabolites involved in some pathways.

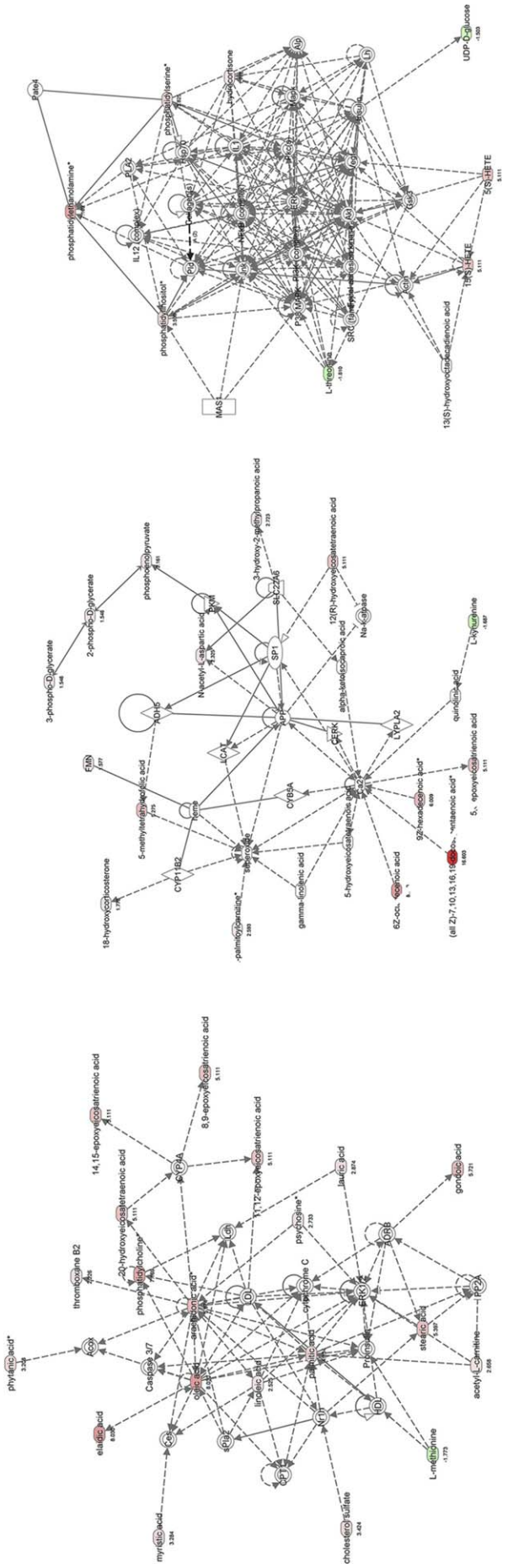

agonist known, with a median effective concentration of 1 nM. Moreover, it has higher selectivity (>1000-fold) over the other two PPAR isoforms [39]. We speculate that the actions of PPARD agonist on placenta likely are PPARD-dependent in the present study.

We demonstrated that *Ppard* activation alters the content and composition of placental lipids. Of the 67 most relevant metabolites, 34 consist of fatty acids. In particular, a significant increase of the main components of polyunsaturated fatty acids was observed, including DPA, EPA, and AA in GW501516-treated groups versus controls. DPA is an intermediate product between EPA and docosahexaenoic acid (DHA). AA and DHA have been implicated in proper fetal brain and eye development [40]. EPA is positively correlated with fatty acid binding protein mRNA expression [41] that, in turn, enables free fatty acid, such as DHA and AA, to cross the placenta to meet the demands of the normal growing fetus, whereas insufficient intake of EPA during pregnancy is associated with preterm birth [42]. Thus, the changes in placental lipid contents caused by GW501516 appear to be involved in the modulation of free fatty acid transport processes.

Previous studies have reported that activation of *Ppard* not only induced gene expression involved in energy production in adipose tissue and skeletal muscle [43, 44] but also significantly improved glucose tolerance and insulin resistance in the animal model of high fat diet-induced obesity [45]. On the other hand, loss of *Ppard* in mouse muscle exhibited reduced oxidative and metabolic efficiency [46]. These studies emphasize the regulatory role of *Ppard* in fatty acid oxidation, energy expenditure, and glucose homeostasis. However, the role of *Ppard* pertaining to placental metabolic activates is not well clarified. Our study revealed that the network most altered by GW501516 involved a highly interconnected carbohydrate and energy metabolism, characterized by up-regulated glycolysis and lipid biosynthesis activities. These results, in agreement with previous reports on the beneficial effects of *Ppard* on lipid metabolism and whole-body glucose tolerance [43–46], implicates that activation of *Ppard* may offer an effective strategy in preventing gestational diabetes by increasing placental capacity for fatty acid oxidation, energy expenditure, and glucose homeostasis. Given the loss of *Ppard* in mice causes induction of embryo lethality as well as reduction of energy uncoupling and adipose mass [25], such effects on placental metabolic activities may also explain the placental malformation outcomes of *Ppard* deficiency.

In addition to its role in transporting molecules between mother and fetus [47], the placenta is a major endocrine organ that provides abundant hormones for mammalian reproductive success [48]. Our finding that *Ppard* activation leads to the augmented sterol lipids, such as desoxycorticosterone acetate (4-fold change) and cholesterol sulfate (3.4-fold change), indicates the involvement of *Ppard* activation in prompting the placental endocrine secretions, which are crucial for placental development and fetal growth. Interestingly, the metabolism analysis showed the positive effects of GW501516 on AA (5.7-fold change), because AA per se is one of the endogenous *Ppard* ligands that not only regulates human chorionic gonadotropin-induced steroidogenesis but also plays

FIG. 5. Metabolite expression regulatory networks predicted by IPA based on the metabolites listed in Table 1. AKT and ERK were predicted to be activated. Each node represents a metabolite. Red nodes denote up-regulated metabolites, and green nodes denote down-regulated metabolites. Dotted lines indicated indirect regulatory interactions, whereas solid lines show direct regulatory interactions.

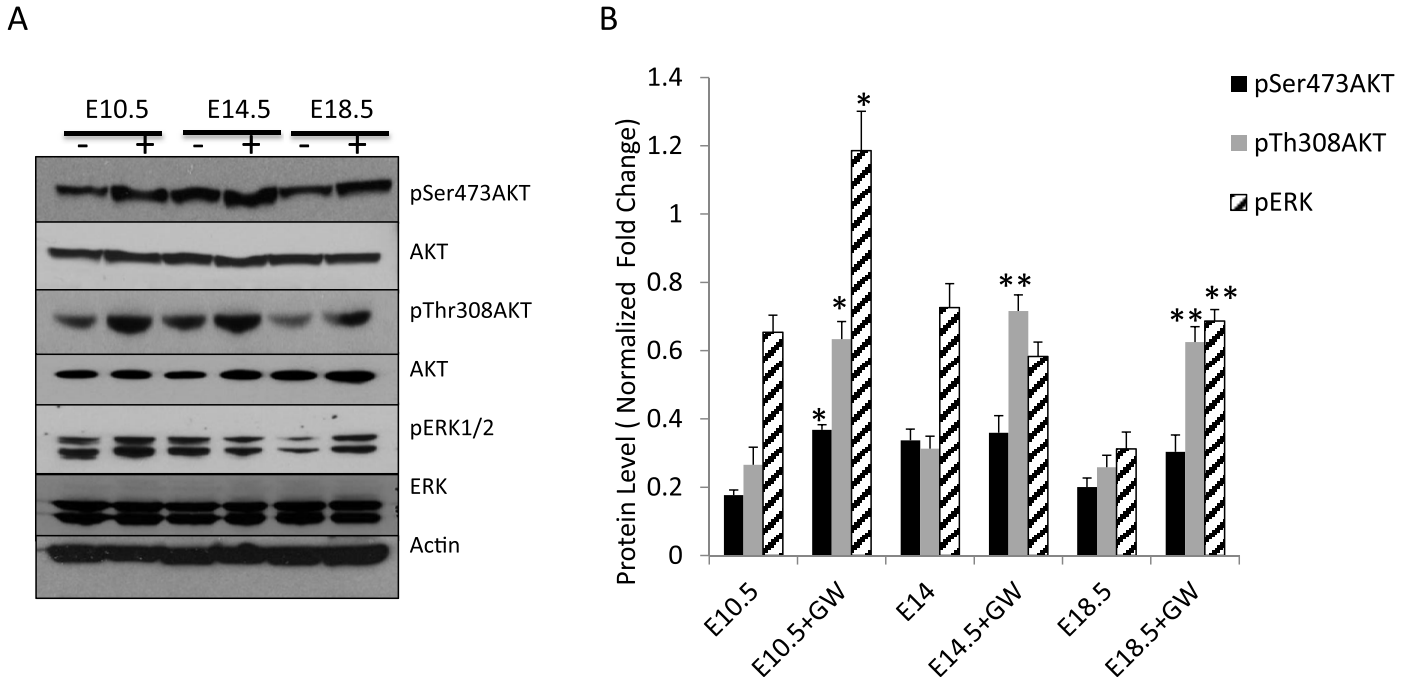

FIG. 6. The effects of *Ppard* agonist on AKT and ERK signaling pathways. **A**) Representative Western blots of the signaling pathways underlying *Ppard* activation in placentas. GW501516 led to significant increase in Th308AKT, Ser473AKT, and ERK phosphorylation. **B**) Bar graph of the ratio of pTh308AKT/AKT, pSer473AKT/AKT, and pERK1/2/ERK1/2 shown in **A**. All values are normalized to actin. Each value represents the mean ± SD, expressed relative to control values. Student *t*-test was performed on the data. $^{**}P < 0.01$, $^{*}P < 0.05$ denotes significant differences between GW501516-treated versus control groups.

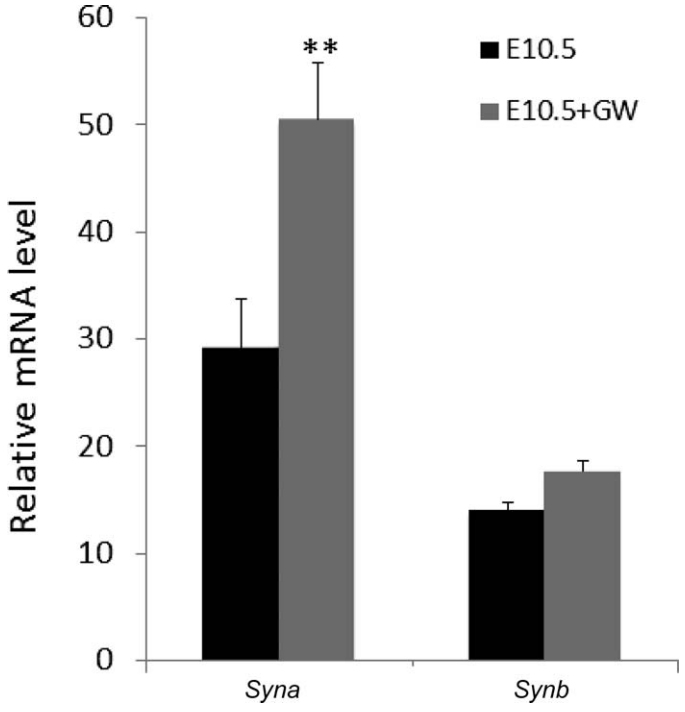

FIG. 7. The effects of *Ppard* agonist on syncytin expression. The qPCR analysis of the placental cytotrophoblast differentiation markers *syna* and *synb* gene expression is shown. *Syna* significantly increased in GW501516-treated placenta in comparison to control mice, whereas no significant change was found in *Synb* expression (n = 6 mice/group) between the two groups. The data represent the mean ± SD. $^{**}P < 0.01$ denotes significant differences between GW501516-treated versus control groups.

a role in testosterone formation in rat Leydig cells [49, 50]. Thus, the increased AA in the present study may explain why *Ppard* activation confers placental endocrine system development and placentation.

Furthermore, our analysis of biology function predicted that *Ppard* might positively regulate AKT and ERK signaling pathways mediated by metabolites during pregnancy. In agreement with the network analysis from IPA, the Western blot analysis showed that *Ppard* activation resulted in an increase of pTh308AKT, pSer473AKT, and pERK1/2 expression. Although the direct mechanical link between *Ppard* activation and AKT/ERK signaling is missing, our metabolomics profiling suggests that *Ppard* activation leads to elevated levels of fatty acids, which presumably drive the activation of the AKT indirectly through the PI3K/PDK1/AKT axis [51] and the phosphorylation of ERK through the EGFR/ERK/p90RSK pathway [52]. Notably, 15(S)-HETE is a downstream product of AA and enhances the expression of placental growth factor through PI3/AKT signaling pathway [53]. Moreover, the interaction between *Ppard* and PI3K/AKT signaling was found in other cell types [54, 55]. Given that *Ppard* is a fatty acid sensor in regulating lipid metabolism in several metabolic tissues [56], the present study provides a molecular mechanical linking between *Ppard* and AKT/ERK activities in the placenta metabolic processes.

Syncytin, a fusogenic glycoprotein of endogenous retroviral origin, plays a critical role in the regulation of cytotrophoblast differentiation [57]. Among the PPAR family, the role of PPARG in regulating syncytin-1 mRNA expression as well as trophoblast differentiation and invasion is well established [58, 59]. However, *Ppard* effects on cytotrophoblast differentiation in placentas are unknown. Our data show that GW501516 increased *Syna,* but not *Synb,* mRNA expression, suggesting that *Ppard* activation positively regulates cytotrophoblast differentiation. Because the formation of syncytium coincided

with glycolysis and energy production during cytotrophoblast differentiation [60], we speculate that the role of *Ppard* activation is regulating *Syna* expression via the modulation of metabolic pathway, which was reflected by induced glycolysis upon GW501516 treatment. In addition, as the 5′-long terminal repeat of human endogenous retrovirus-W (HERV-W) promoter contains three putative PPAR response elements (PPREs 1–3), which suggests that *Ppard* may directly regulate *Syn* transcription [59]. Thus, the effect of *Ppard* activation in promoting cytotrophoblasts differentiation merits further attention.

In summary, our data suggest that *Ppard* activation is associated with changes of lipid content in the placenta that correspond with unregulated AKT/ERK signaling pathways and *Syna* expression. Further studies in human placenta are needed to better understand the impact of altered metabolic functions of *Ppard* activation on placental development, fetal growth, and the cellular mechanisms involved.

ACKNOWLEDGMENT

We are grateful to Dr. Xirong Guo for help with the present study. We thank Dr. Jinlian Wang for data analysis.

REFERENCES

1. Rossant J, Cross JC. Placental development: lessons from mouse mutants. Nat Rev Genet 2001; 2:538–548.
2. Leiser R, Kaufmann P. Placental structure: in a comparative aspect. Exp Clin Endocrinol 1994; 102:122–134.
3. Morrish DW, Dakour J, Li H. Functional regulation of human trophoblast differentiation. J Reprod Immunol 1998; 39:179–195.
4. Cross JC. Placental function in development and disease. Reprod Fertil Dev 2006; 18:71–76.
5. Cole LA. New discoveries on the biology and detection of human chorionic gonadotropin. Reprod Biol Endocrinol 2009; 7:8.
6. Coleman RA, Haynes EB. Synthesis is and release of fatty acids by human trophoblast cells in culture. J Lipid Res 1987; 28:1335–1341.
7. Peng L, Payne AH. AP-2gamma and the homeodomain protein distal-less 3 are required for placental-specific expression of the murine 3beta-hydroxysteroid dehydrogenase VI gene, *Hsd3b6*. J Biol Chem 2002; 277: 7945–7954.
8. Shalom-Barak T, Zhang X, Chu T, Timothy Schaiff W, Reddy JK, Xu J, Sadovsky Y, Barak Y. Placental PPARγ regulates spatiotemporally diverse genes and a unique metabolic network. Dev Biol 2012; 372: 143–155.
9. Martínez N, Capobianco E, White V, Pustovrh MC, Higa R, Jawerbaum A. Peroxisome proliferator-activated receptor alpha activation regulates lipid metabolism in the feto-placental unit from diabetic rats. Reproduction 2008; 136:95–103.
10. Barak Y, Sadovsky Y, Shalom-Barak T. PPAR signaling in placental development and function. PPAR Res 2008; 142082.
11. Krey G, Braissant O, L'Horset F, Kalkhoven E, Perroud M, Parker MG, Wahli W. Fatty acids, eicosanoids, and hypolipidemic agents identified as ligands of peroxisome proliferator-activated receptors by coactivator-dependent receptor ligand assay. Mol Endocrinol 1997; 11:779–791.
12. Naruhn S, Meissner W, Adhikary T, Kaddatz K, Klein T, Watzer B, Müller-Brüsselbach S, Müller R. 15-Hydroxyeicosatetraenoic acid is a preferential peroxisome proliferator-activated receptor beta/delta agonist. Mol Pharmacol 2010; 77:171–184.
13. Sznaidman ML, Haffner CD, Maloney PR, Fivush A, Chao E, Goreham D, Sierra ML, LeGrumelec C, Xu HE, Montana VG, Lambert MH, Willson TM, et al. Novel selective small molecule agonists for peroxisome proliferator-activated receptor delta (PPARdelta)—synthesis and biological activity. Bioorg Med Chem Lett 2003; 13:1517–1521.
14. Wang YX, Zhang CL, Yu RT, Cho HK, Nelson MC, Bayuga-Ocampo CR, Ham J, Kang H, Evans RM. Regulation of muscle fiber type and running endurance by PPARdelta. PLoS Biol 2004; 2:e294.
15. Schmuth M, Haqq CM, Cairns WJ, Holder JC, Dorsam S, Chang S, Lau P, Fowler AJ, Chuang G, Moser AH, Brown BE, Mao-Qiang M, et al. Peroxisome proliferator-activated receptor (PPAR)-beta/delta stimulates differentiation and lipid accumulation in keratinocytes. J Invest Dermatol 2004; 122:971–983.
16. Vrins CL, van der Velde AE, van den Oever K, Levels JH, Huet S, Oude Elferink RP, Kuipers F, Groen AK. Peroxisome proliferator-activated receptor delta activation leads to increased transintestinal cholesterol efflux. J Lipid Res 2009; 50:2046–2054.
17. Bastie C, Holst D, Gaillard D, Jehl-Pietri C, Grimaldi PA. Expression of peroxisome proliferator-activated receptor PPARdelta promotes induction of PPARgamma and adipocyte differentiation in 3T3C2 fibroblasts. J Biol Chem 1999; 274:21920–21925.
18. Piqueras L, Reynolds AR, Hodivala-Dilke KM, Alfranca A, Redondo JM, Hatae T, Tanabe T, Warner TD, Bishop-Bailey D. Activation of Ppard induces endothelial cell proliferation and angiogenesis. Arterioscler Thromb Vasc Biol 2007; 27:63–69.
19. Piqueras L, Sanz MJ, Perretti M, Morcillo E, Norling L, Mitchell JA, Li Y, Bishop-Bailey D. Activation of PPARbeta/delta inhibits leukocyte recruitment, cell adhesion molecule expression, and chemokine release. J Leukoc Biol 2009; 86:115–122.
20. Coll T, Rodrïguez-Calvo R, Barroso E, Serrano L, Eyre E, Palomer X, Vázquez-Carrera M. Peroxisome proliferator-activated receptor (PPAR) beta/delta: a new potential therapeutic target for the treatment of metabolic syndrome. Curr Mol Pharmacol 2009; 2:46–55.
21. Michalik L, Desvergne B, Dreyer C, Gavillet M, Laurini RN, Wahli W. PPAR expression and function during vertebrate development. Int J Dev Biol 2002; 46:105–114.
22. Wang Q, Fujii H, Knipp GT. Expression of PPAR and RXR isoforms in the developing rat and human term placentas. Placenta 2002; 23:661–671.
23. Wang H, Xie H, Sun X, Tranguch S, Zhang H, Jia X, Wang D, Das SK, Desvergne B, Wahli W, DuBois RN, Dey SK. Stage-specific integration of maternal and embryonic peroxisome proliferator-activated receptor delta signaling is critical to pregnancy success. J Biol Chem 2007; 282: 37770–37782.
24. Kang HJ, Hwang SJ, Yoon JA, Jun JH, Lim HJ, Yoon TK, Song H. Activation of peroxisome proliferators-activated receptor delta (PPARdelta) promotes blastocyst hatching in mice. Mol Hum Reprod 2010; 17: 653–660.
25. Barak Y, Liao D, He W, Ong ES, Nelson MC, Olefsky JM, Boland R, Evans RM. Effects of peroxisome proliferator-activated receptor delta on placentation, adiposity, and colorectal cancer. Proc Natl Acad Sci U S A 2002; 99:303–308.
26. Nadra K, Anghel SI, Joye E, Tan NS, Basu-Modak S, Trono D, Wahli W, Desvergne B. Differentiation of trophoblast giant cells and their metabolic functions are dependent on peroxisome proliferator-activated receptor beta/delta. Mol Cell Biol 2006; 26:3266–3281.
27. Kurtz M, Capobianco E, Martínez N, Fernández J, Higa R, White V, Jawerbaum A. Carbaprostacyclin, a PPARdelta agonist, ameliorates excess lipid accumulation in diabetic rat placentas. Life Sci 2010; 86:781–790.
28. Capobianco E, Martínez N, Fornes D, Higa R, Di Marco I, Basualdo MN, Faingold MC, Jawerbaum A. PPAR activation as a regulator of lipid metabolism, nitric oxide production and lipid peroxidation in the placenta from type 2 diabetic patients. Mol Cell Endocrinol 2013; 377:7–15.
29. Tautenhahn R, Patti GJ, Rinehart D, Siuzdak G. XCMS Online: a web-based platform to process untargeted metabolomic data. Anal Chem 2012; 84:5035–5039.
30. Patti GJ, Tautenhahn R, Siuzdak G. Meta-analysis of untargeted metabolomic data from multiple profiling experiments. Nat Protoc 2012; 7:508–516.
31. Zhou B, Wang J, Ressom HW. MetaboSearch: tool for mass-based metabolite identification using multiple databases. PLoS ONE 2012; 7: e40096.
32. Wishart DS, Tzur D, Knox C, Eisner R, Guo AC, Young N, Cheng D, Jewell K, Arndt D, Sawhney S, Fung C, Nikolai L, et al. HMDB: the Human Metabolome Database. Nucleic Acids Res 2007; 35:D521–D526.
33. Tautenhahn R, Cho K, Uritboonthai W, Zhu Z, Patti GJ, Siuzdak G. An accelerated workflow for untargeted metabolomics using the METLIN database. Nat Biotechnol 2012; 30:826–828.
34. Krueger R, Le Buanec B. Action needed to harmonize regulation of low-level presence of biotech traits. Nat Biotechnol 2008; 26:161–162.
35. Park JY, Park BK, Ko JS, Bang S, Song SY, Chung JB. Bile acid analysis in biliary tract cancer. Yonsei Med J 2006; 47:817–825.
36. Larqué E, Ruiz-Palacios M, Koletzko B. Placental regulation of fetal nutrient supply. Curr Opin Clin Nutr Metab Care 2013; 16:292–297.
37. Wang WS, Liu C, Li WJ, Zhu P, Li JN, Sun K. Involvement of CRH and hCG in the induction of aromatase by cortisol in human placental syncytiotrophoblasts. Placenta 2014; 35:30–36.
38. Nishimura K, Nakano N, Chowdhury VS, Kaneto M, Torii M, Hattori MA, Yamauchi N, Kawai M. Effect of PPARβ/δ agonist on the placentation and embryo-fetal development in rats. Birth Defects Res B Dev Reprod Toxicol 2013; 98:164–169.
39. Oliver WR Jr, Shenk JL, Snaith MR, Russell CS, Plunket KD, Bodkin NL,

Lewis MC, Winegar DA, Sznaidman ML, Lambert MH, Xu HE, Sternbach DD, et al. A selective peroxisome proliferator-activated receptor delta agonist promotes reverse cholesterol transport. Proc Natl Acad Sci U S A 2001; 98:5306–5311.
40. Ramakrishnan U, Stein AD, Parra-Cabrera S, Wang M, Imhoff-Kunsch B, Juarez-Marquez S, Rivera J, Martorell R. Effects of docosahexaenoic acid supplementation during pregnancy on gestational age and size at birth: randomized, double-blind, placebo-controlled trial in Mexico. Food Nutr Bull 2010; 31:S108–S116.
41. Larqué E, Krauss-Etschmann S, Campoy C, Hartl D, Linde J, Klingler M, Demmelmair H, Caño A, Gil A, Bondy B, Koletzko B. Docosahexaenoic acid supply in pregnancy affects placental expression of fatty acid transport proteins. Am J Clin Nutr 2006; 84:853–861.
42. Olsen SF, Østerdal ML, Salvig JD, Weber T, Tabor A, Secher NJ. Duration of pregnancy in relation to fish oil supplementation and habitual fish intake: a randomized clinical trial with fish oil. Eur J Clin Nutr 2007; 61:976–985.
43. Dressel U, Allen TL, Pippal JB, Rohde PR, Lau P, Muscat GE. The peroxisome proliferator-activated receptor beta/delta agonist, GW501516, regulates the expression of genes involved in lipid catabolism and energy uncoupling in skeletal muscle cells. Mol Endocrinol 2003; 17:2477–2493.
44. Roberts LD, Murray AJ, Menassa D, Ashmore T, Nicholls AW, Griffin JL. The contrasting roles of PPARdelta and PPARgamma in regulating the metabolic switch between oxidation and storage of fats in white adipose tissue. Genome Biol 2011; 12:R75.
45. Tanaka T, Yamamoto J, Iwasaki S, Asaba H, Hamura H, Ikeda Y, Watanabe M, Magoori K, Ioka RX, Tachibana K, Watanabe Y, Uchiyama Y, et al. Activation of peroxisome proliferator-activated receptor delta induces fatty acid beta-oxidation in skeletal muscle and attenuates metabolic syndrome. Proc Natl Acad Sci U S A 2003; 100:15924–15929.
46. Schuler M, Ali F, Chambon C, Duteil D, Bornert JM, Tardivel A, Desvergne B, Wahli W, Chambon P, Metzger D. PGC1alpha expression is controlled in skeletal muscles by PPARbeta, whose ablation results in fiber-type switching, obesity, and type 2 diabetes. Cell Metab 2006; 4: 407–414.
47. Burton GJ, Fowden AL. The placenta and developmental programming: balancing fetal nutrient demands with maternal resource allocation. Placenta 2012; 33:S23–S27.
48. Maslar IA, Hess DL, Buckmaster JG, Lazur JJ, Stanczyk FZ, Novy MJ. Steroid production by early pregnancy human placental villi in culture. Placenta 1990; 11:277–288.
49. Didolkar AK, Sundaram K. Arachidonic acid is involved in the regulation of hCG induced steroidogenesis in rat Leydig cells. Life Sci 1987; 41: 471–477.
50. Romanelli F, Valenca M, Conte D, Isidori A, Negro-Vilar A. Arachidonic acid and its metabolites effects on testosterone production by rat Leydig cells. J Endocrinol Invest 1995; 18:186–193.
51. Shibata E, Kanno T, Tsuchiya A, Kuribayashi K, Tabata C, Nakano T, Nishizaki T. Free fatty acids inhibit protein tyrosine phosphatase 1B and activate Akt. Cell Physiol Biochem 2013; 32:871–879.
52. Nikolakopoulou Z, Nteliopoulos G, Michael-Titus AT, Parkinson EK. Omega-3 polyunsaturated fatty acids selectively inhibit growth in neoplastic oral keratinocytes by differentially activating ERK1/2. Carcinogenesis 2013; 34:2716–2725.
53. Wu MY, Yang RS, Lin TH, Tang CH, Chiu YC, Liou HC, Fu WM. Enhancement of PLGF production by 15-(S)-HETE via PI3K-Akt, NF-κB and COX-2 pathways in rheumatoid arthritis synovial fibroblast. Eur J Pharmacol 2013; 714:388–396.
54. Tian XY, Wong WT, Wang N, Lu Y, Cheang WS, Liu J, Liu L, Liu Y, Lee SS, Chen ZY, Cooke JP, Yao X, et al. PPARδ activation protects endothelial function in diabetic mice. Diabetes 2012; 61:3285–3293.
55. Han JK, Lee HS, Yang HM, Hur J, Jun SI, Kim JY, Cho CH, Koh GY, Peters JM, Park KW, Cho HJ, Lee HY, et al. Peroxisome proliferator-activated receptor-delta agonist enhances vasculogenesis by regulating endothelial progenitor cells through genomic and nongenomic activations of the phosphatidylinositol 3-kinase/Akt pathway. Circulation 2008; 118: 1021–1033.
56. Wang YX, Lee CH, Tiep S, Yu RT, Ham J, Kang H, Evans RM. Peroxisome-proliferator-activated receptor delta activates fat metabolism to prevent obesity. Cell 2003; 113:159–170.
57. Henke C, Ruebner M, Faschingbauer F, Stolt CC, Schaefer N, Lang N, Beckmann MW, Strissel PL, Strick R. Regulation of murine placentogenesis by the retroviral genes *Syncytin-A, Syncytin-B* and *Peg10*. Differentiation 2013; 85:150–160.
58. Ruebner M, Langbein M, Strissel PL, Henke C, Schmidt D, Goecke TW, Faschingbauer F, Schild RL, Beckmann MW, Strick R. Regulation of the human endogenous retroviral syncytin-1 and cell-cell fusion by the nuclear hormone receptors PPARγ/RXRα in placentogenesis. J Cell Biochem 2012; 113:2383–2389.
59. Levytska K, Drewlo S, Baczyk D, Kingdom J. PPAR-γ regulates trophoblast differentiation in the BeWo cell model. PPAR Res 2014; 2014:637251.
60. Bax BE, Bloxam DL. Energy metabolism and glycolysis in human placental trophoblast cells during differentiation. Biochim Biophys Acta 1997; 1319:283–292.